



Online monitoring of printed electronics by Spectral-Domain Optical Coherence Tomography

Erkki Alarousu, Ahmed AlSaggaf & Ghassan E. Jabbour

Solar and Photovoltaics Engineering Research Center, King Abdullah University of Science and Technology, 4700 King Abdullah University of Science and Technology, Thuwal 23955-6900, Saudi Arabia.

SUBJECT AREAS:
IMAGING TECHNIQUES
CHARACTERIZATION AND
ANALYTICAL
TECHNIQUES
IMAGING AND SENSING
OPTICAL METROLOGY

Received
7 January 2013

Accepted
13 March 2013

Published
28 March 2013

Correspondence and requests for materials should be addressed to E.A. (erkki.alarousu@kaust.edu.sa) or G.E.J. (ghassanjabbour1@gmail.com)

Spectral-Domain Optical Coherence Tomography (SD-OCT) is an optical method capable of 3D imaging of object's internal structure with micron-scale resolution. Modern SD-OCT tools offer the speed capable of online monitoring of printed devices. This paper demonstrates the use of SD-OCT in a simulated roll-to-roll (R2R) process through monitoring some structural properties of moving screen printed interdigitated electrodes. It is shown that structural properties can be resolved for speeds up to ca. 1 m/min, which is the first step towards application of this method in real manufacturing processes, including roll-to-roll (R2R) printing.

High speed printing, including R2R, have gained significant attention in recent years due to their potential in the fabrication of low cost electronics, photonics, and energy harvesting devices^{1,2}. Printing techniques such as screen printing³, gravure printing⁴, and ink jet printing⁵⁻¹⁰ have been successfully used in the fabrication of flexible solar cells, light emitting diodes, and other devices. It is important in such approaches to have a real time capability that allows a noninvasive inspection of structural properties of printed features, without interrupting the printing speed. Among such properties are thickness, line width, roughness, homogeneity, and defects such as voids, which need to be evaluated frequently in a device manufacturing process. The thickness and line width of different layers depend on the intended function of the layer and the materials at hand. In research based R2R printing, thickness ranging from 0.01 to 100 micron, minimum line width from 10 to 100 micron and printing speed from 0.02 to 25 m/min have been reported¹¹⁻¹⁵. Table 1 summarizes such parameters.

Currently, the evaluation of some structural properties of printed devices is done by analyzing images taken either by a high speed camera (noninvasive) or by traditional characterization tools that require a full interruption of the process for physically removing the sample. Among the candidates that may be suitable for online inspection in a R2R process is the powerful and promising OCT.

OCT is a broad technique including time-domain¹⁶, spectral-domain¹⁷, swept-source¹⁸, full-field¹⁹, etc. The majority of OCT applications are in medical fields such as ophthalmology²⁰, dermatology²¹, and gastroenterology²², to mention a few. Several nonmedical applications of OCT have been recently reviewed by *Stifter*²³. Such applications include characterization of ceramics, glasses, optical components, polymers, fiber composites, paper, archaeological science, art diagnostics and microfluidics. *Fujiwara et al.* used swept-source OCT to perform cross sectional online imaging of security features in paper based documents²⁴. Electrical components characterization by OCT was first introduced by *Scmitt*²⁵ who demonstrated the use of OCT in imaging of GaAlAs LED encapsulated in epoxy. Recent study by *Cho et al.*²⁶ shows the offline application of OCT in screening defects in LED manufacturing process. The first study demonstrating the application of OCT in printed functional materials and printed electronics was published by *Czajkowski et al.* in 2010²⁷. The authors applied ultra-high resolution time-domain OCT (UHR TD-OCT) to evaluate the internal structure of epoxy embedded RF-antenna. The same group published later the use of UHR TD-OCT to study encapsulation quality of Parylene C coated organic field effect transistor²⁸. *Thrane et al.* demonstrated the use of TD-OCT in imaging the multilayer structure and identifying defects of R2R coatings in a polymer solar cells²⁹.

For device applications, 3D structural imaging in R2R process requires relatively fast (video-rate) and accurate (micron resolution) capturing of images. It is difficult to combine these two parameters in one tool, especially for a resolution approaching one to few micrometers. While fast video-rate SD-OCT has been demonstrated in ophthalmology^{30,31}, its use in printed electronics and photonics has been lacking. In this work, we demonstrate for the first



Table 1 | Printing methods along with typical research and pilot line-type relevant parameters^{11–15,32,33}

Method	Minimum line width (μm)	Ink layer thickness (μm)	Printing speed (m/min)
Flexography	30–80	0.04–8	1–25
Gravure	10–50	0.02–12	0.2–25
Rotary screen	50–100	1–100	0.04–2
InkJet	10–50	0.01–0.5	0.02–5

time, to the best of our knowledge, the use of SD-OCT to monitor printed device structural properties of a moving sample. We will show that it is possible with this approach to obtain several structural properties of silver based printed interdigitated electrodes.

Results

Electrodes were first measured by a Brüker Contour GT-X optical profilometer to get a reference for online SD-OCT measurements and information about the dimensions of the print. Fig. 1 shows the 3D topography including X- and Y-profiles of the electrodes. X-profile stands for machine direction (MD) i.e. the direction of sample, or web movement in case of R2R, while Y-profile represents the cross direction (CD), i.e. perpendicular to the movement.

Translation stage speeds from 0 to 1.50 m/min, with 0.15 m/min steps, were used to demonstrate the dynamic imaging capability of SD-OCT. Fig. 2 shows 3D reconstruction of the electrodes including slice images in MD and CD taken from an actual measurement for speeds of 0, 0.45, 0.75 and 1.50 m/min. Avizo® software was used to reconstruct 3D volumes from raw data. Data or image processing e.g. smoothing or correction of pixel positions due to target movement during image recording was not involved in the reconstruction phase. Fig. 3 shows a comparison between SD-OCT and optical profilometer data. SD-OCT image is overlaid by profilometer image with varying opacity from 0% to 100%, from left to right, to illustrate the correlation of data sets.

As can be seen, the pattern measured by SD-OCT is clearly recognizable for all four speed values and matches well with the optical profilometer data. It's worth mentioning that 1.50 m/min is the highest speed attainable by the translation stage used in this study. However, image quality deteriorates with further increase in speed due to increasing pixel pitch in MD, which is already 88.4 μm at 1.50 m/min speed, causing the structure to become blurred and

dimensions in MD less accurate. Electrode and gap widths derived from the slice in MD direction (turquoise line in Fig. 2) and two adjacent slices on opposite sides $\pm 280 \mu\text{m}$ apart, give an average value with standard deviation shown in Table 2.

We can see from the data that after 1.05 m/min, the pixel pitch in MD becomes too large (61.8 μm) compared to the size of the measured feature, rendering it difficult to resolve the dimensions accurately. However, the data in CD do not change for all speeds. In the z-direction, measurements are taken continuously with a frequency of 127 kHz enabling high speed surface detection with depth resolution of 2.73 μm and 2.73 $\mu\text{m}/n$ for buried surfaces where n is the refractive index of the imaged material.

Discussion

As demonstrated, SD-OCT is a promising method for noninvasive 3D inspection of moving sample of printed devices. As an example, a flexible PET plastic substrate with screen printed silver-based interdigitated electrodes was translated at various speeds while under inspection by SD-OCT, simultaneously. We showed that the printed structures could be resolved with a resolution of 29 μm in CD (pixel pitch used). Moreover, depending on speed, an 8.8 μm – 88.4 μm resolution in MD was obtained. Resolution in MD is a result of multiplying the translational speed of the stage by the time taken to record one image in CD, which was ca. 3.5 ms. Due to the limited depth resolution of the setup used, the topography of the electrodes could not be evaluated.

As presented in Table 2, dimensions can be resolved up to speed of 1.05 m/min, after which the pixel pitch becomes too large in MD compared to the measured feature size causing inaccurate measurement.

As a conclusion, we have demonstrated the use of 3D SD-OCT to image moving interdigitated electrodes at speeds ranging from 0 to 1.50 m/min, and proved that device structural properties can be obtained online with high resolution up to ca. 1 m/min. For higher speed processes, our current SD-OCT demonstration can be extended by incorporating relatively higher acquisition rate camera, faster beam deflection optomechanics, as well as faster ability to process and save large amount of data in shorter time frame. In addition to speed, high resolution is important when imaging printed structures. To enhance the resolution into submicron region, high power ultra-broadband light source based on supercontinuum generation (wavelength from 400 nm to 2 μm) can be used. Furthermore, the results presented in this work can be viewed as a first step towards demonstrating the potential of SD-OCT as an

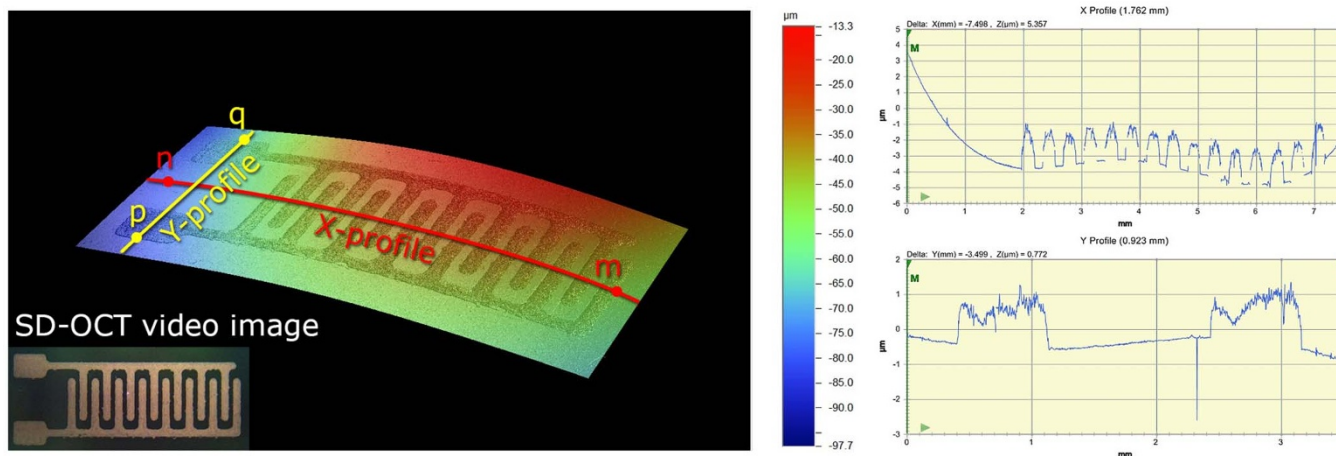


Figure 1 | 3D topography and SD-OCT video image of electrodes (left). Substrate has a little curvature in MD and tilt in CD which are corrected on the profiles (right) to enhance the visibility of single electrode. Average electrode thickness is 1.5–2.5 μm and width 230 μm . Total length [mm] of a given electrode is 6.85 mm in MD and width [mm] 2.77 mm in CD.

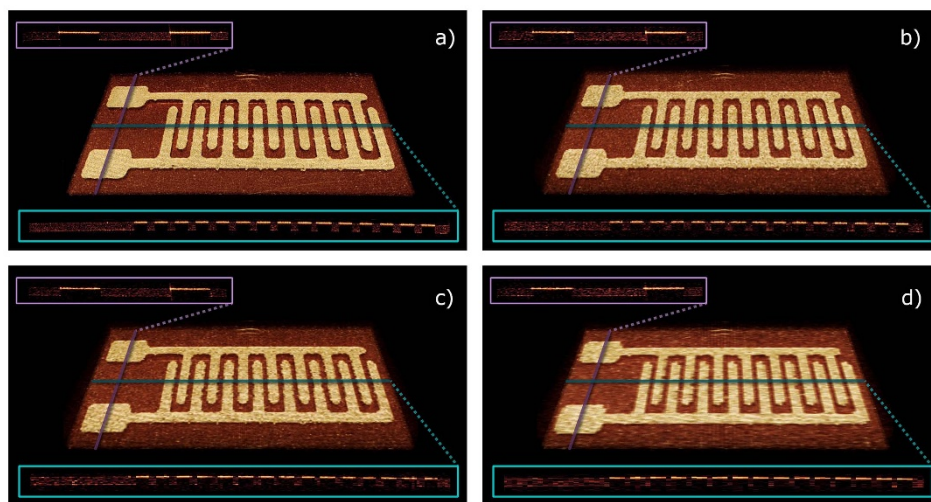


Figure 2 | 3D reconstruction of the printed interdigitated electrodes moving with varying speed. (a) Stationary sample has $700 \times 346 \times 123$ pixels in 3D, each pixel has a size of $10.4 \mu\text{m} \times 10.4 \mu\text{m} \times 2.73 \mu\text{m}$, (b) sample moving at a speed of 0.45 m/min has $276 \times 123 \times 131$ pixels in 3D, each pixel has a size of $26.5 \mu\text{m} \times 29 \mu\text{m} \times 2.73 \mu\text{m}$, (c) sample moving at 0.75 m/min has $166 \times 123 \times 131$ pixels in 3D, each pixel has a size of $44.2 \mu\text{m} \times 29 \mu\text{m} \times 2.73 \mu\text{m}$ and (d) electrodes moving at 1.50 m/min has $83 \times 122 \times 129$ pixels in 3D, each pixel has a size of $88.4 \mu\text{m} \times 29 \mu\text{m} \times 2.73 \mu\text{m}$. Violet and turquoise boxes represent slice images in CD and MD direction, respectively. The slice images were taken from the actual 3D data and not measured separately.

online structural inspection tool in R2R printed processes of functional layers and devices.

Methods

An interdigitated electrodes structure with 40% of silver nanoparticles screen printed on a flexible PET plastic substrate was obtained from PChem. Thorlabs Hyperion SD-OCT tool was used in the acquisition of 3D images of stationary and moving electrodes. A-scan (one scan in the vertical direction) is performed with a frequency of

127 kHz. In the case of 125 A-scans (1 mm depth/367 pixels) in the cross-sectional image, recording was performed with 283 Hz frame rate based on time taken to record spectral data, apodization cycles, and resetting the galvanometric scanners for stable operation. Depth resolution (z direction) of the tool is $5.8 \mu\text{m}/n$, where n is the refractive index of the imaged material. This value is calculated from the coherence length of the light source and defines the resolving capability of two scatterers close to each other in z direction. On the other hand, resolving the position of a single scatterer in depth, e.g. an interface, is determined by the pixel spacing in the vertical direction which is in this case $2.73 \mu\text{m}/n$. Transversal resolution (xy direction) is $8 \mu\text{m}$ which is

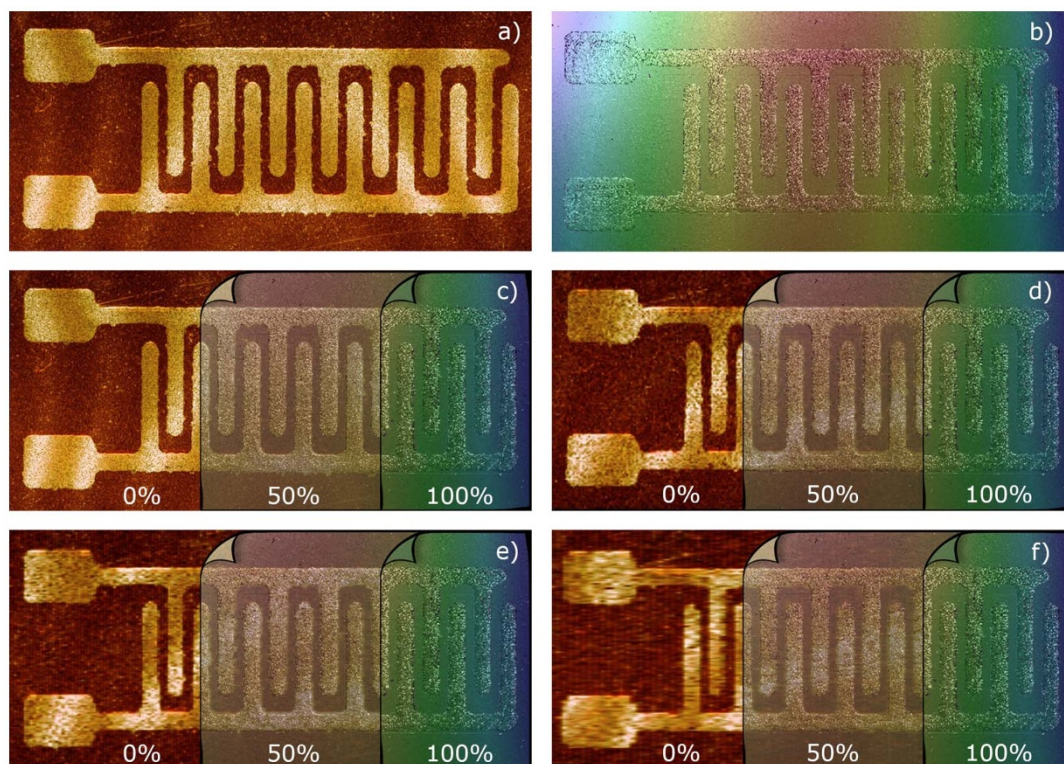


Figure 3 | Comparison of data acquired by SD-OCT and Brükler ContourGT-X optical profilometer. (a) Topview of SD-OCT tomography data at 0 m/min speed, (b) topview of the ContourGT-X profilometer data. Profilometer data overlaying SD-OCT results with 0%, 50% and 100% opacity at speeds, (c) 0 m/min, (d) 0.45 m/min, (e) 0.75 m/min and (f) 1.50 m/min, respectively.



Table 2 | Average width of electrodes and gaps with standard deviations for different speeds

Speed (m/min)	Average width of electrode (μm)	Average width of gap (μm)
0	231 \pm 13	124 \pm 13
0.15	232 \pm 13	121 \pm 13
0.30	232 \pm 16	122 \pm 14
0.45	228 \pm 17	125 \pm 16
0.60	233 \pm 22	121 \pm 21
0.75	231 \pm 31	125 \pm 29
0.90	227 \pm 27	126 \pm 29
1.05	232 \pm 33	119 \pm 21
1.20	209 \pm 26	145 \pm 22
1.35	216 \pm 44	140 \pm 46
1.50	261 \pm 18	93 \pm 19

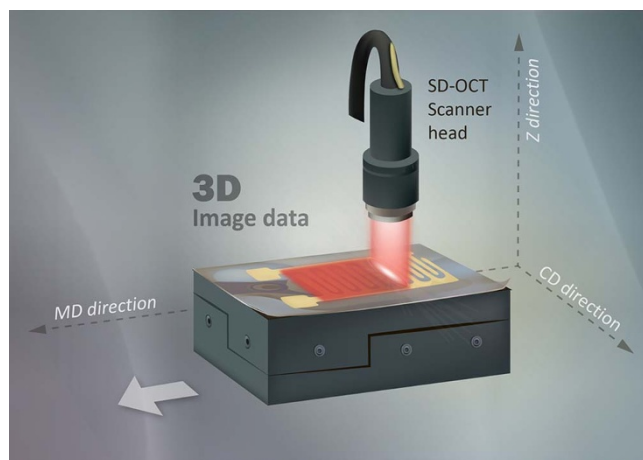


Figure 4 | Measurement sequence for 3D image reconstruction.

defined by the imaging optics. The printed interdigitated electrode sample was mounted on a DC-servo motor based precision translation stage driven by a high-performance motion controller. The stage has a maximum speed of 25 mm/s. The sample was tilted 6° in CD to avoid saturation of the camera, and to achieve highest sensitivity. The sample was moved at constant speed in machine direction (MD) during image recording. SD-OCT tool was set to scan a length of 3.625 mm line with 125 A-scans in CD which, gives 29 μm pixel pitch. Fig. 4 shows 3D measurement sequence used in this study. 283 Hz frame rate was achieved with this approach which yields 8.8 μm –88.4 μm pixel pitch in MD when the stage speed was varied between 0.15 m/min–1.50 m/min.

1. Logothetidis, S. Flexible organic electronic devices: Materials, process and applications. *Mater Sci Eng B-Adv* **152**, 96–104 (2008).
2. Krebs, F. C. Fabrication and processing of polymer solar cells: A review of printing and coating techniques. *Sol Energ Mat Sol C* **93**, 394–412 (2009).
3. Jabbour, G. E., Radspinner, R. & Peyghambarian, N. Screen printing for the fabrication of organic light-emitting devices. *Ieee J Sel Top Quant* **7**, 769–773 (2001).
4. Kopola, P. *et al.* Gravure printed flexible organic photovoltaic modules. *Sol Energ Mat Sol C* **95**, 1344–1347 (2011).
5. de Gans, B. J., Duineveld, P. C. & Schubert, U. S. Inkjet Printing of Polymers: State of the Art and Future Developments. *Adv Mater* **16**, 203–213 (2004).
6. Singh, M., Haverinen, H. M., Dhagat, P. & Jabbour, G. E. Inkjet Printing-Process and Its Applications. *Adv Mater* **22**, 673–685 (2010).
7. Haverinen, H. M., Myllyla, R. A. & Jabbour, G. E. Inkjet printing of light emitting quantum dots. *Applied Physics Letters* **94** (2009).
8. Haverinen, H. M., Myllyla, R. A. & Jabbour, G. E. Inkjet Printed RGB Quantum Dot-Hybrid LED. *J Disp Technol* **6**, 87–89 (2010).
9. Wunscher, S. *et al.* Localized atmospheric plasma sintering of inkjet printed silver nanoparticles. *J Mater Chem* **22**, 24569–24576 (2012).
10. Smith, P. J., Shin, D. Y., Stringer, J. E., Derby, B. & Reis, N. Direct ink-jet printing and low temperature conversion of conductive silver patterns. *J Mater Sci* **41**, 4153–4158 (2006).

11. Chun, S. *et al.* Roll-to-Roll Printing of Silver Oxide Pastes and Low Temperature Conversion to Silver Patterns. *Chem Mater* **21**, 343–350 (2009).
12. Espinosa, N. *et al.* Life cycle assessment of ITO-free flexible polymer solar cells prepared by roll-to-roll coating and printing. *Sol Energ Mat Sol C* **97**, 3–13 (2012).
13. Han, M. G. *et al.* Polyaniline coated poly(butyl methacrylate) core-shell particles: roll-to-roll printing of templated electrically conductive structures. *J Mater Chem* **17**, 1347–1352 (2007).
14. Huebner, C. F. *et al.* Electroluminescent colloidal inks for flexographic roll-to-roll printing. *J Mater Chem* **18**, 4942–4948 (2008).
15. Kang, H., Lee, C. & Shin, K. A novel cross directional register modeling and feedforward control in multi-layer roll-to-roll printing. *J Process Contr* **20**, 643–652 (2010).
16. Huang, D. *et al.* Optical Coherence Tomography. *Science* **254**, 1178–1181 (1991).
17. Fercher, A. F., Hitzinger, C. K., Kamp, G. & Elzaiat, S. Y. Measurement of Intraocular Distances by Backscattering Spectral Interferometry. *Opt Commun* **117**, 43–48 (1995).
18. Chinn, S. R., Swanson, E. A. & Fujimoto, J. G. Optical coherence tomography using a frequency-tunable optical source. *Opt Lett* **22**, 340–342 (1997).
19. Dubois, A., Vabre, L., Boccara, A. C. & Beaulieu, E. High-resolution full-field optical coherence tomography with a Linnik microscope. *Appl Optics* **41**, 805–812 (2002).
20. Drexler, W. *et al.* Ultrahigh-resolution ophthalmic optical coherence tomography. *Nat Med* **7**, 502–507 (2001).
21. Pierce, M. C., Strasswimmer, J., Park, B. H., Cense, B. & de Boer, J. F. Advances in optical coherence tomography imaging for dermatology. *J Invest Dermatol* **123**, 458–463 (2004).
22. Zuccaro, G. *et al.* Optical coherence tomography (OCT) characterization of Barrett's esophagus (BE). *Am J Gastroenterol* **95**, 2443–2444 (2000).
23. Stifter, D. Beyond biomedicine: a review of alternative applications and developments for optical coherence tomography. *Appl Phys B-Lasers O* **88**, 337–357 (2007).
24. Fujiwara, K. & Matoba, O. High-speed cross-sectional imaging of valuable documents using common-path swept-source optical coherence tomography. *Appl Optics* **50**, H165–H170 (2011).
25. Schmitt, J. M. Compact in-Line Interferometer for Low-Coherence Reflectometry. *Opt Lett* **20**, 419–421 (1995).
26. Cho, N. H., Jung, U., Kim, S. & Kim, J. Non-Destructive Inspection Methods for LEDs Using Real-Time Displaying Optical Coherence Tomography. *Sensors-Basel* **12**, 10395–10406 (2012).
27. Czajkowski, J., Prykari, T., Alarousu, E., Palosaari, J. & Myllyla, R. Optical coherence tomography as a method of quality inspection for printed electronics products. *Opt Rev* **17**, 257–262 (2010).
28. Czajkowski, J. *et al.* Ultra-high resolution optical coherence tomography for encapsulation quality inspection. *Appl Phys B-Lasers O* **105**, 649–657 (2011).
29. Thrane, L., Jorgensen, T. M., Jorgensen, M. & Krebs, F. C. Application of optical coherence tomography (OCT) as a 3-dimensional imaging technique for roll-to-roll coated polymer solar cells. *Sol Energ Mat Sol C* **97**, 181–185 (2012).
30. Szkulmowski, M. *et al.* Quality improvement for high resolution in vivo images by spectral domain optical coherence tomography with supercontinuum source. *Opt Commun* **246**, 569–578 (2005).
31. Nassif, N. A. *et al.* In vivo high-resolution video-rate spectral-domain optical coherence tomography of the human retina and optic nerve. *Optics Express* **12**, 367–376 (2004).
32. Lee, T. M., Lee, S. H., Noh, J. H., Kim, D. S. & Chun, S. The effect of shear force on ink transfer in gravure offset printing. *J Micromech Microeng* **20** (2010).
33. Siden, J. & Nilsson, H. E. Line width limitations of flexographic- screen- and inkjet printed RFID antennas. *Ieee Antennas Prop*, 1596–1599 (2007).

Acknowledgments

We would like to thank Christian Winters (Thorlabs GmbH) for valuable information about Hyperion parameters.

Author contributions

E.A. designed and performed the experiments. A.A. assisted in some of the experiments. E.A. and G.E.J. discussed the results. E.A., A.A. and G.E.J. wrote the paper. G.E.J. supervised the work.

Additional information

Competing financial interests: The authors declare no competing financial interests.

License: This work is licensed under a Creative Commons Attribution-NonCommercial-NoDerivs 3.0 Unported License. To view a copy of this license, visit <http://creativecommons.org/licenses/by-nc-nd/3.0/>

How to cite this article: Alarousu, E., AlSaggaf, A. & Jabbour, G.E. Online monitoring of printed electronics by Spectral-Domain Optical Coherence Tomography. *Sci. Rep.* **3**, 1562; DOI:10.1038/srep01562 (2013).